

Author's Accepted Manuscript

Enhanced ductility in dynamic strain aging regime
in a Fe-25Ni-20Cr austenitic stainless steel

Abdullah S. Alomari, N. Kumar, K.L. Murty



PII: S0921-5093(18)30718-4
DOI: <https://doi.org/10.1016/j.msea.2018.05.060>
Reference: MSA36498

To appear in: *Materials Science & Engineering A*

Received date: 8 April 2018
Revised date: 17 May 2018
Accepted date: 18 May 2018

Cite this article as: Abdullah S. Alomari, N. Kumar and K.L. Murty, Enhanced ductility in dynamic strain aging regime in a Fe-25Ni-20Cr austenitic stainless steel, *Materials Science & Engineering A*, <https://doi.org/10.1016/j.msea.2018.05.060>

This is a PDF file of an unedited manuscript that has been accepted for publication. As a service to our customers we are providing this early version of the manuscript. The manuscript will undergo copyediting, typesetting, and review of the resulting galley proof before it is published in its final citable form. Please note that during the production process errors may be discovered which could affect the content, and all legal disclaimers that apply to the journal pertain.

Enhanced ductility in dynamic strain aging regime in a Fe-25Ni-20Cr austenitic stainless steel

Abdullah S. Alomari^{a,b}, N. Kumar^a, K.L. Murty^{a,*}

^aDepartment of Nuclear Engineering, North Carolina State University, Raleigh, NC, USA

^bAtomic Energy Research Institute, King Abdulaziz City for Science and Technology, Riyadh, Saudi Arabia

*murty@ncsu.edu

Abstract

Contrary to the commonly observed embrittlement during dynamic strain aging, we report in this note distinct enhancement in ductility in a Nb-containing and nitrogen stabilized Fe-25(wt.%)Ni-20Cr austenitic stainless steel (Alloy 709) at temperatures from 623 K to 873 K at 10^{-4} s^{-1} where serrated flow is noted. This observation is rationalized in terms of the influence of strain hardening parameters and strain rate sensitivity on uniform elongation and ductility respectively.

Keywords: Ductility, Austenitic steels, Dynamic strain aging, High temperature deformation

In both interstitial and substitutional solid solution alloys, stress-strain curves during tensile deformation exhibit serrations known as Portevin-Le Chatelier effect (PLE) within a specific regime of temperature and strain rate [1, 2]. The phenomenon is commonly attributed to a macroscopic observation of dynamic strain aging (DSA) resulting from the interaction between moving dislocations and solute atoms during deformation. Dislocations in a crystalline material move in intermittent way during plastic deformation. At elevated temperatures, solute atoms diffuse to the core of mobile dislocations during waiting time at obstacles and pin them leading to repeated locking and unlocking of the mobile dislocations during plastic deformation that give rise to serrated stress–strain curves [3-5]. Other indicators of the occurrence of DSA include peaks and/or plateaux of the flow stresses, decreased or negative strain rate sensitivity and

minima in ductility [1, 2]. DSA has been shown to cause an adverse effect on other mechanical properties of materials such as fatigue life [6] and fracture toughness [7], in addition to ductility [8-12]. It is believed that the detrimental effect of serrated flow on ductility is caused by the decreased strain rate sensitivity [5]. The embrittlement effect of DSA which is similar to the blue brittleness in ferritic steels is of importance since many engineering materials operate at the temperature range of DSA [13].

Ductility loss in DSA regime during tensile deformation has been numerously reported for various metals including ferritic steels [11], austenitic stainless steels [12], Al-based alloys [10], Ti-based alloys [8], and Zr-based alloys [9]. Contrary to this commonly observed detrimental effect, we report here a significant improvement in ductility during the DSA phenomenon in Alloy 709, a Nb-containing and nitrogen stabilized Fe-25Ni-20Cr austenitic stainless steel at temperatures ranging from 623 K to 873 K (350 to 600 °C) where serrated flow is observed.

The material investigated in this study is a highly alloyed austenitic stainless steel (Alloy 709) which is a candidate structural material for next generation sodium fast reactors due to its excellent mechanical properties relative to conventional austenitic stainless steels such as SS304 and SS316 [14]. The Alloy 709 was received in the form of hot forged rectangular bar annealed at 1373 K (1100 °C) for 2 hours followed by water-quenching with the following chemical composition (wt. %) - C: 0.063, Mn: 0.88, Si: 0.28, P: <0.005, S: <0.001, Cr: 19.9, Ni: 25, Mo: 1.46, N: 0.14, Ti: <0.01, Nb: 0.23, B: 0.0022, and the rest being Fe. The average grain size was determined to be $36.8 \pm 7.3 \mu\text{m}$ using line intercept method. Rectangular pin-loaded tensile specimens with gage length of 20 mm were machined from the as-received plate and were tested using an Instron Universal tester equipped with a three-zone furnace at a constant cross-head velocity. Tensile tests were performed at a wide range of temperatures varying from 298 K to

1073 K (25 to 800 °C) and at two nominal strain rates of 10^{-3} s^{-1} and 10^{-4} s^{-1} . The temperature was maintained within $\pm 1 \text{ K}$ ($\pm 1 \text{ }^{\circ}\text{C}$) and the soaking time for each sample was kept at 30 min for tests at each temperature. Tensile tests at 10^{-3} s^{-1} were repeated (2 to 3 times) to ensure the reproducibility of the tensile test data. The average values are reported with error bars corresponding to the standard deviations. The force and extension data during tensile tests were recorded using a load cell and LVDT installed on the testing machine. The microstructure of the as-received and deformed samples was characterized by Transmission Electron Microscopy (TEM) using a JEOL 2000FX S/TEM operated at an accelerating voltage of 200 kV.

Typical engineering stress-engineering strain curves of the Alloy 709 as function of temperatures at a strain rate of 10^{-3} s^{-1} are shown in Figure 1. The alloy exhibits serrated flow during tensile deformation at intermediate temperatures depending on the strain rate. At a strain rate of 10^{-3} s^{-1} , serrations were found to be in the temperature range 573–973 K (300–700 °C) whereas it was confined in the range 523–923 K (250–650 °C) at 10^{-4} s^{-1} . For each stress-strain curve, the serrated flow commences after a finite amount of plastic deformation and continues until fracture occurs.

The variations of 0.2% yield strength (YS) and the ultimate tensile strength (UTS) with temperature are shown in Figure 2. To emphasize the influence of temperature on strength values, normalized YS and UTS by Young's modulus are considered. The values of Young's modulus, E at various temperatures for the Alloy 709 have been obtained from $E=6,895(28.73-0.01T)$ where E is in MPa and the temperature, T in °C for a 20%Cr-25%Ni-Nb stabilized austenitic stainless steel [15]. At both strain rates, a slight decrease in the normalized UTS from 298–373 K (25–100 °C) is observed followed by a peak at intermediate temperatures before it rapidly decreases at higher temperatures. The variation of the normalized YS exhibits a

significant decrease with increase in temperature from 298–473 K (25–200 °C) followed by a plateau or slight peak depending on the strain rate at intermediate temperatures. With further increase in the temperature, a moderate decrease in YS is observed at both strain rates. It is noted that the peaks and plateaux observed in the YS and UTS coincided very well with the occurrence of serrated flow regime.

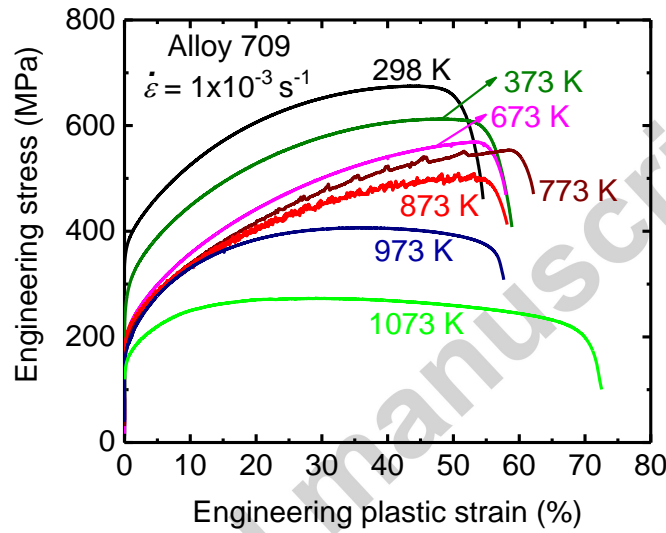


Figure 1. Engineering stress – engineering strain curves at a strain rate of $1 \times 10^{-3} \text{ s}^{-1}$ at different temperatures

Also shown in Figure 2 are the temperature variations of ductility defined as the elongation-to-fracture, ϵ_f , uniform elongation, ϵ_u (*i.e.* elongation up to maximum load in an engineering stress – engineering strain curve) and non-uniform elongation, ϵ_{nu} (*i.e.* post-uniform elongation or necking strain defined as $\epsilon_{nu} = \epsilon_f - \epsilon_u$). A slight decrease in ϵ_f with temperature ranging from 298–673 K (25–400 °C) is found before a significant peak is observed at 773 K (500 °C) in serrated flow regime followed by a rapid increase at high temperatures. Further, the variations of ϵ_u and ϵ_{nu} with temperature are also included in Figure 2, and ϵ_u shows no significant variation with temperature up to 673 K (400 °C) followed by a pronounced peak at around 773 K (500 °C) before a sharp decrease at higher temperatures. Unlike the ϵ_f , the ϵ_{nu} exhibits a slow decrease

from 298–573 K (25–300 °C) followed by a wide minimum at intermediate temperatures 573–873 K (300–600 °C) followed by a sharp increase at high temperatures.

The microstructure of the Alloy 709 before testing is shown in Figure 3(a) where relatively low dislocation density and some preexisting fine precipitates of less than 200 nm are typically observed. Figure 3(b) shows a TEM image of the Alloy 709 strained to failure at a temperature of 573 K (300 °C) and strain rate of 10^{-3} s^{-1} within the DSA regime where a high degree of planarity of dislocation glide is noted. The observed linear dislocation substructure was pronounced as a manifestation of deformation by planar slip of dislocations restricting the cross-slip and recovery due to DSA at intermediate temperatures [16]. For comparison, Figure 3(c) includes a TEM image of the alloy deformed at 373 K (100 °C) (outside DSA regime) showing non-planar arrangement of dislocation substructure.

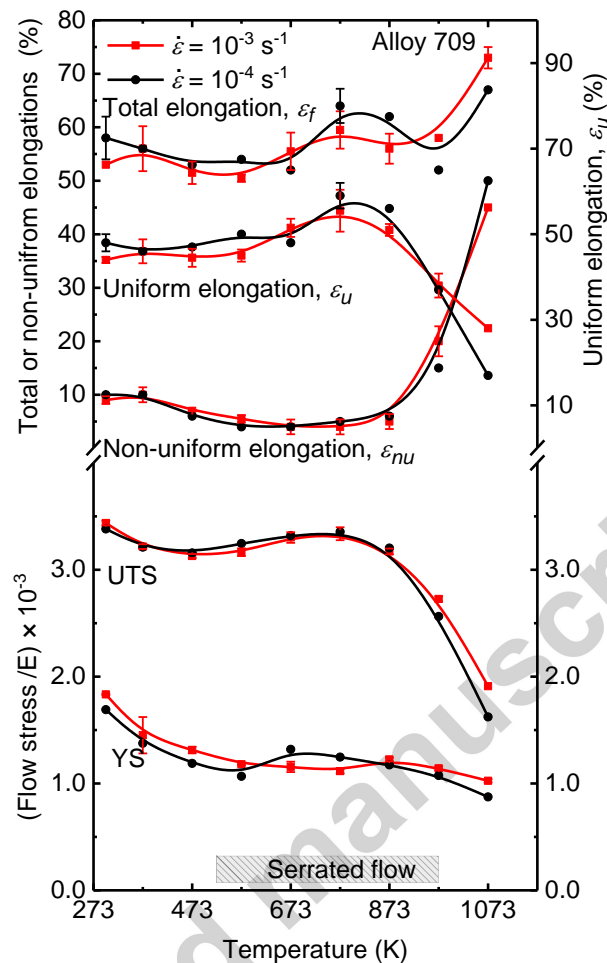


Figure 2. Effect of test temperature on yield (YS) and tensile strengths (UTS) as well as ductility (ϵ_f), uniform (ϵ_u) and non-uniform (ϵ_{nu}) elongations at two different strain rates

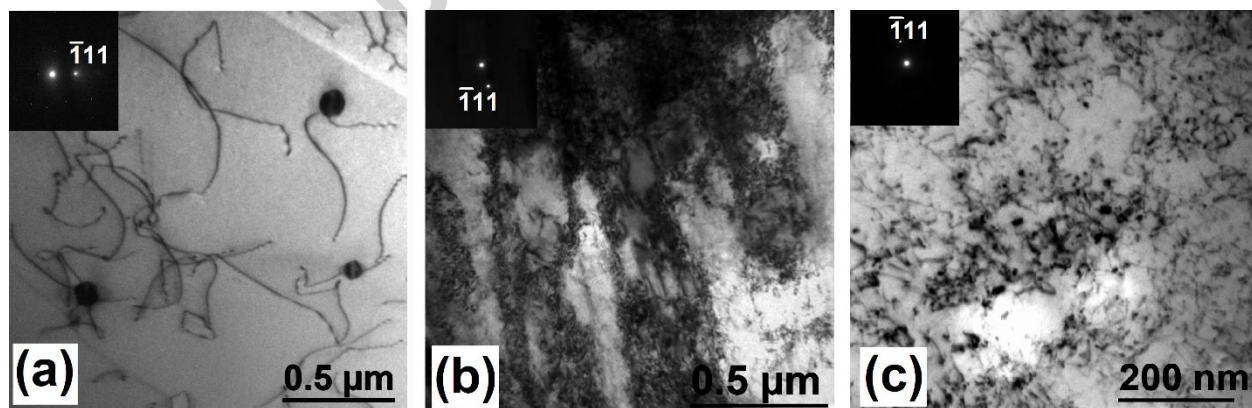
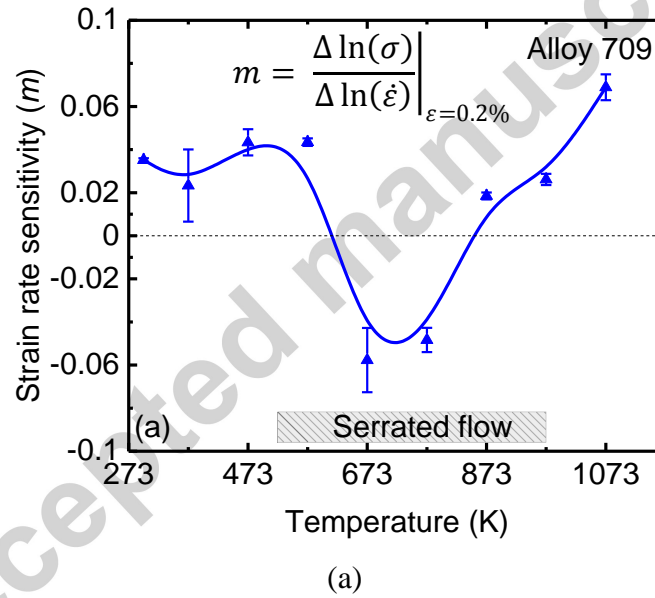


Figure 3. (a) Bright field TEM image for the undeformed Alloy 709, (b) the deformed Alloy 709 at temperature of 573 K and strain rate of 10^{-3} s^{-1} (DSA regime), and (c) the deformed Alloy 709 at temperature of 373 K and strain rate of 10^{-3} s^{-1} (non-DNA regime). The insets show corresponding selected area diffraction patterns.

The temperature-strain rate regime for the occurrence of serrated flow and the observed peaks/plateaux of the YS and UTS in the Alloy 709 are consistent with the observations reported for various austenitic stainless steels where the diffusivity of solute atoms is comparable to the average velocity of the mobile dislocations during tensile deformation [17, 18]. In SS316L(N) austenitic stainless steel, Choudhary reported minima in elongation-to-fracture at temperatures ranging from 523–873 K (250–600 °C) and related this effect to the negative strain rate sensitivity observed in this regime [12]. In type AISI 316 steel, Almeida and Monteiro have reported a constant uniform elongation inside the DSA range [19]. They attributed this behavior to the large work hardening rate in DSA regime. In mild steel, the change in the work hardening characteristics of the material in the DSA temperature range leading to the onset of necking at small strains was suggested to be responsible for the loss in ductility [20]. In contrast, we note here a pronounced peak in serrated flow regime for the total and uniform elongations at both strain rates in the Alloy 709.

To develop better understanding about this contradictory observation in the Alloy 709, the strain rate sensitivity (m), the strain hardening exponent (n) and work hardening rate (θ) are examined. The strain rate sensitivity (m) is determined from the equation: $m = \ln(\sigma_1 / \sigma_2) / \ln(\dot{\epsilon}_1 / \dot{\epsilon}_2)$ where σ_1 and σ_2 are flow stresses at strain rates of 10^{-3} and 10^{-4} s^{-1} respectively. The values of m as a function of temperature are shown in Figure 4(a) where negative strain rate sensitivity is clearly observed in the serrated flow regime. In the absence of DSA, strain rate sensitivity is reported to increase monotonically with temperature inhibiting the growth of localized deformation after necking resulting in high ductility [5]. A proportional relationship between elongation to fracture and strain rate sensitivity is well established in many metals and alloys [21]. In DSA regime, solute atoms diffuse to the mobile dislocations and pin

them enhancing the localized deformation leading to a negative strain rate sensitivity. A decreasing value of m in DSA regime would mean diminishing tendency toward preventing localized deformation resulting therefore in decreased ductility. The reduction in non-uniform elongation in the Alloy 709 at intermediate temperatures can be explained by the negative strain sensitivity found in DSA regime. After the neck formation, the failure is enhanced due to the low m -value. On the other hand, the strain hardening behavior during deformation is a key factor influencing the ductility, particularly the uniform elongation since strain hardening exponent (n) is equal to true uniform strain: $n = \varepsilon_u$.



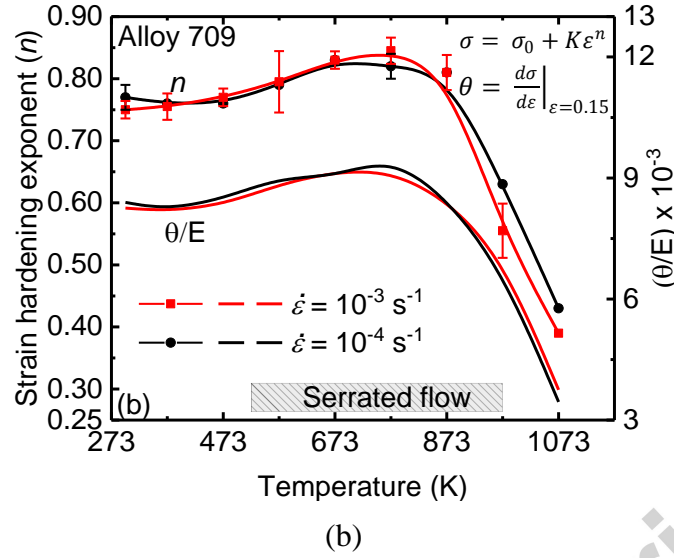


Figure 4 a. Strain rate sensitivity (m) vs temperature. b. Temperature variations of strain hardening exponent (n) (left scale) and normalized work-hardening rate (θ/E) at true plastic strain of 0.15 at two different strain rates

A high value of strain hardening exponent will enhance the uniform elongation which might also improve the overall ductility [22]. To estimate the strain hardening exponent in the Alloy 709, true stress- true strain curves up to the point of necking were curve-fitted using the least square fit with Ludwik's equation: $\sigma = \sigma_0 + K\epsilon^n$ where σ_0 , K and n are constants representing yield stress, strain hardening coefficient and strain hardening exponent respectively; the correlation coefficients, R^2 for all fitting curves, were higher than 0.98. Figure 4(b) shows the values of n as a function of temperature at different strain rates in the Alloy 709 where a significant peak in the strain hardening exponent is observed in the serrated flow regime depicting the increase in the uniform elongation (Figure. 2). Similarly, the work-hardening rate, θ (where θ is defined as the first derivative of the Ludwik's equation) is influenced by the occurrence of DSA. The variations of the normalized work-hardening rate, θ/E at true plastic strain of 0.15 with temperature at different strain rates are also shown in Figure 4(b), and θ/E exhibits peaks at intermediate temperatures where serrated flow occurs. Consequently, the net

effect was a ductility enhancement in the DSA regime due to the relatively large uniform strain while the negative strain sensitivity was not sufficient to form the necking earlier. Further investigation into this observation and a detailed microstructural evaluation is underway and will be reported along with further details on kinetics of DSA such as the activation energy and correlations between the strain-rate and strain.

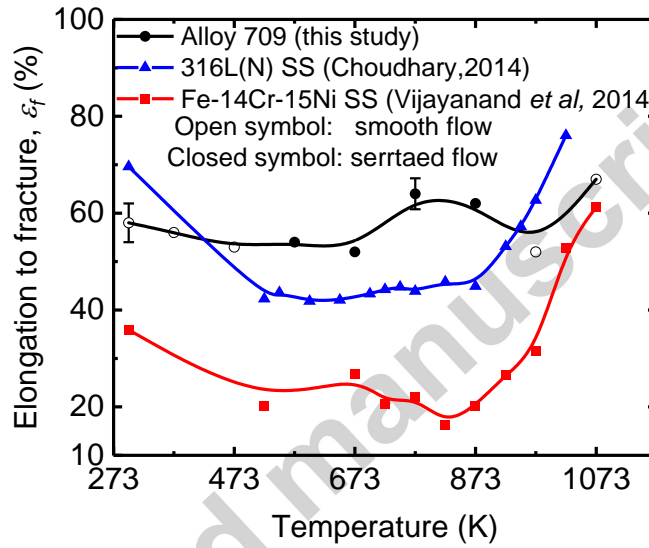


Figure 5. Temperature variation of ductility in Alloy 709 vs SS

It is interesting to compare the current results on Alloy 709 with those reported for 316SS [12] and Fe-14%Cr-15Ni SS [23] and figure 5 summarizes the total elongation to fracture for these alloys where the enhanced ductility during DSA in the Alloy 709 is clearly demonstrated. Recently, Calmunger et al. reported improved ductility of a highly alloyed austenitic stainless steel within the DSA regime and concluded that both high Ni content and deformation twinning govern the better ductility within DSA [24]. The Alloy 709 has a relatively large amount of Ni which may have bearing on work hardening parameters n and θ responsible for the enhancement of the uniform elongation and hence the ductility in DSA regime.

In summary, the serrated flow in the stress-strain curves were observed in an austenitic stainless steel (Alloy 709) at temperatures ranging from 523–973 K (250–700 °C) and at two nominal strain rates of 10^{-3} and 10^{-4} s $^{-1}$. Although the peaks/plateaux in the YS and UTS and negative strain sensitivity were observed in the serrated flow regime, increased ductility is noted in lieu of ductility minima commonly reported. This contradictory observation was attributed to the increase in the strain hardening exponent and work hardening rate in dynamic strain aging regime illustrating the fact that DSA is not always detrimental to metals [25].

Acknowledgments

The authors gratefully acknowledge the financial support from the Nuclear Energy University Programs (NEUP) of the Department of Energy, Office of Nuclear Energy for performing this research and Dr. Sam Sham of Argonne National Laboratory for various discussions and the experimental material.

References

- [1] P. Rodriguez, Serrated plastic flow, *Bull. Mater. Sci.* 6 (1984) 653-663.
- [2] J.M. Robinson, M.P. Shaw, Microstructural and mechanical influences on dynamic strain aging phenomena, *Int. Mater. Rev.* 39 (1994) 113-122.
- [3] P.G. McCormick, A model for the Portevin-Le Chatelier effect in substitutional alloys, *Acta Metall.* 20 (1972) 351-354.
- [4] A. van den Beukel, Theory of the effect of dynamic strain aging on mechanical properties, *Phys. Status Solidi A* 30 (1975) 197-206.
- [5] L.P. Kubin, Y. Estrin, Dynamic strain ageing and the mechanical response of alloys, *J. Phys.* III 1 (1991) 929-943.
- [6] V.S. Srinivasan, M. Valsan, R. Sandhya, K. Bhanu Sankara Rao, S.L. Mannan, D.H. Sastry, High temperature time-dependent low cycle fatigue behaviour of a type 316L(N) stainless steel, *Int. J. Fatigue* 21(1) (1999) 11-21.
- [7] Y.H. Jung, K.L. Murty, Effect of Temperature and Strain Rate on Upper Shelf Fracture Behavior of A533B Class 1 Pressure Vessel Steel, in: T.A. Cruse (Ed.), *Fracture Mechanics: Nineteenth Symposium*, ASTM, STP 969, Philadelphia, 1988, pp. 392-401.
- [8] M. Doner, H. Conrad, Deformation mechanisms in commercial Ti (0.5 at. pct oineq) at intermediate and high temperatures (0.3 - 0.6 tinm), *Metall. Trans.* 4 (1973) 2809-2817.
- [9] S.I. Hong, W.S. Ryu, C.S. Rim, Elongation Minimum and Strain Rate Sensitivity Minimum of Zircaloy-4 *J. Nucl. Mater.* 116 (1983) 314-316.

- [10] E. Bouchaud, L. Kubin, H. Octor, Ductility and dynamic strain aging in rapidly solidified aluminum alloys, *Metall. Trans. A* 22 (1991) 1021-1028.
- [11] C. Gupta, J.K. Chakravartty, S.L. Wadekar, J.S. Dubey, Effect of serrated flow on deformation behaviour of AISI 403 stainless steel, *Mater. Sci. Eng., A* 292 (2000) 49-55.
- [12] B.K. Choudhary, Influence of Strain Rate and Temperature on Tensile Deformation and Fracture Behavior of Type 316L(N) Austenitic Stainless Steel, *Metall. Mater. Trans. A* 45 (2014) 302-316.
- [13] K.L. Murty, E.O. Hall, Dynamic Strain-Aging and Neutron Irradiation in Mild Steel in: *Irradiation Effects on the Microstructure and Properties of Metals*, ASTM STP 611, 1976, pp. 53-71.
- [14] T.-L. Sham, L. Tan, Y. Yamamoto, Development of Advanced 9Cr Ferritic-Martensitic Steels and Austenitic Stainless Steels for Sodium-Cooled Fast Reactors, in: *Fast Reactors and Related Fuel Cycles: Safe Technologies and Sustainable Scenarios (FR13)*, IAEA, Vienna, 2015, pp. 1-9.
- [15] E.G. Wilson, Stress varied creep of 20%Cr-25%Ni-Nb stabilized austenitic stainless steel, *Creep strength in steel and high temperature alloys*, The Metal Society, London, 1972, pp. 111-121.
- [16] W. Karlsen, M. Ivanchenko, U. Ehrnstén, Y. Yagodzinskyy, H. Hänninen, Microstructural manifestation of dynamic strain aging in AISI 316 stainless steel, *J. Nucl. Mater.* 395(1) (2009) 156-161.
- [17] L.H.D. Almeida, I.L. May, S.N. Monteiro, Effects of Carbon and Nitrogen Levels on the Temperature Ranges for Serrated Flow in Austenitic Stainless Steel, in: H.J. McQueen, J.P. Bailon, J.I. Dickson, J.J. Jonas, M.G. Akben (Eds.), *Strength of Metals and Alloys (ICSMA 7)*, Pergamon Press, Oxford, 1985, pp. 337-342.
- [18] V. Ganesan, K. Laha, M. Nandagopal, P. Parameswaran, M.D. Mathew, Effect of nitrogen content on dynamic strain ageing behaviour of type 316LN austenitic stainless steel during tensile deformation, *Mater. High Temp.* 31 (2014) 162-170.
- [19] L.H.d. Almeida, S.N. Monteiro, The Significance of Dynamic Strain Aging in Austenitic Stainless Steel, in: *Proceedings of the second International Conference on Mechanical Behavior of Materials*, ASM, Metals Park, 1976, pp. 1697-1701.
- [20] B.J. Brindley, The Effect of Dynamic Strain Ageing on the Ductile Fracture Process in Mild Steel, *Acta Metall.* 18 (1970) 325-329.
- [21] D.W. Woodfrod, Strain rate sensitivity as a measure of ductility, *Trans. ASM* 62 (1969) 291-293.
- [22] K.L. Murty, I. Charit, *An Introduction to Nuclear Materials : Fundamentals and Applications*, Wiley-VCH, Weinheim, 2013.
- [23] V.D. Vijayanand, K. Laha, P. Parameswaran, M. Nandagopal, S. Panneer Selvi, M.D. Mathew, Influence of thermo-mechanical treatment on the tensile properties of a modified 14Cr–15Ni stainless steel, *J. Nucl. Mater.* 453 (2014) 188-195.
- [24] M. Calmunger, G. Chai, R. Eriksson, S. Johansson, J.J. Moverare, Characterization of Austenitic Stainless Steels Deformed at Elevated Temperature, *Metall. Mater. Trans. A* 48 (2017) 4525-4538.
- [25] M. Srinivas, G. Malakondaiah, K.L. Murty, P.R. Rao, Fracture toughness in the dynamic strain ageing regime, *Scr. Metall. Mater.* 25 (1991) 2585-2588.